

How Primordial Black Holes Change BBN

Tianning Wang,¹ Evan Grohs,² Laura Mersini-Houghton¹

¹Department of Physics and Astronomy, UNC-Chapel Hill, NC, USA.

²Department of Physics, North Carolina State University, NC, USA.

E-mail: tnwang@unc.edu, ebgrohs@ncsu.edu, mersini@physics.unc.edu

Abstract. Primordial Black Holes (PBHs) provide a powerful probe of early-universe physics, linking inflationary fluctuations to observable cosmological phenomena. In this work, we use a bottom-up approach to study how PBHs with masses in the range $10^8 \leq M \leq 10^{13}$ g modify Big Bang Nucleosynthesis (BBN) through Hawking radiation. We incorporate PBH evaporation into a reaction-network code to evaluate its impact on light-element abundances. Our analysis shows that PBH evaporation acts as an entropy injection mechanism, increasing the comoving entropy density. To reproduce the observed comoving entropy density per baryon (s/n_b) from the CMB, BBN simulations must therefore begin with a smaller initial entropy than in the standard scenario without PBHs. The results also reveal a threshold near $M \approx 10^{10}$ g that separates two distinct regimes of BBN behavior. As an example, for $M \geq 10^{10}$ g, the ${}^4\text{He}$ mass fraction Y_P increases monotonically with β , driven by the enhanced Hubble expansion from PBH energy density. In contrast, for $M \leq 10^{10}$ g, Y_P exhibits non-monotonic behavior shaped by the timing of PBH evaporation and its influence on nuclear reaction rates. These findings highlight the sensitivity of BBN to PBH evaporation and establish a framework for understanding how PBH populations influence the thermal history of the early universe.

Contents

1	INTRODUCTION	1
2	THE FORMATION OF PRIMORDIAL BLACK HOLES	2
3	THE PRIMORDIAL BLACK HOLE MASS FRACTION	3
4	CHANGE IN BBN FROM PBH DECAY	6
5	RESULTS	10
5.1	Entropy and Primordial Abundances	10
5.2	Distinct BBN Behavior Across the Threshold	13
6	SUMMARY AND CONCLUSION	16

1 INTRODUCTION

There has been a growing interest in the study of Primordial Black Holes (PBHs) within the fields of astrophysics and cosmology. Unlike supermassive black holes, which form from the collapse of massive stars, PBHs originate from primordial density fluctuations and are thus of cosmological origin. The diversity in their possible masses motivates the investigation of alternative formation mechanisms for lower-mass black holes. Formed in the early universe, PBHs may arise through various processes generating primordial inhomogeneities [1–16].

Although the existence of PBHs remains speculative, their wide mass spectrum and potential abundances make them compelling candidates for dark matter and, as we show here, for altering the cosmic evolution. This makes them valuable probes of both particle physics and the thermal history [17–26].

Another motivation for studying PBHs is their potential role in the formation of cosmic structures, including galaxies and clusters. Their gravitational influence can attract surrounding matter, facilitating the hierarchical growth of large-scale structures. Theoretical models suggest that PBHs could even serve as seeds of the supermassive black holes observed at galactic centers, merging and accreting mass over cosmic time [27–31].

The aforementioned examples of PBH physics firmly reside in the gravity sector. Past work to include PBHs in cosmology has focused on inducing a change in the Hubble expansion rate: another application of gravitational physics. However, PBHs can and will evaporate in the early universe [32–34]. In essence, PBH evaporation converts mass energy density into radiation. In this work, we will show how the radiation from PBH decay leads to a change in the entropy history of the universe. A change in entropy can have a profound effect on observable data, namely, the primordial element abundances from Big Bang Nucleosynthesis (BBN). Our work here demonstrates a unique connection between gravitation and nuclear physics.

The outline for the remainder of the paper is as follows. To begin, we give a brief review of the early-universe conditions conducive for PBH formation in Sec. 2. We subsequently calculate the PBH mass fraction β using the Green, Liddle, Malik, and Sasaki (GLMS) framework [35] with the inclusion of a running spectral index in Sec. 3. With a model for

β , Sec. 4 details our implementation of Hawking evaporation into a modified version of the BURST nuclear-reaction-network code. We use BURST to evaluate the impact of PBH decay on the synthesis of the light elements ^4He , D, ^3He , and ^7Li . Sec. 5 gives our computational results, which reveal a distinct transition near PBH mass $M \approx 10^{10}$ g. Two distinct regimes of PBH influence on BBN emerge, and we discuss the individual phenomenologies alongside comoving entropy injection from Hawking radiation. We conclude in Sec. 6 with a summary of our findings and a discussion of their broader implications and possible extensions.

2 THE FORMATION OF PRIMORDIAL BLACK HOLES

There is a wide variety of models for the formation of PBH's. Below, we focus on a representative model, as an illustration from which we can estimate the mass spectrum, needed for our purposes. The early universe was a hot, dense plasma dominated by relativistic particles, with the radiation energy density determined by the background temperature as $\rho_{\text{rad}} = \frac{\pi^2}{30} g_* T^4$, where g_* is the relativistic degrees of freedom. From the Friedmann equations, the energy density can also be expressed as $\rho_{\text{rad}} = \frac{3}{8\pi G 4t^2} \approx 4.5 \times 10^5 \left(\frac{1\text{s}}{t}\right)^2 \text{ g cm}^{-3}$. If this radiation density collapsed into a Schwarzschild black hole of radius r_s , it would be natural to compare $M_{\text{rad}} = \rho_{\text{rad}} V_s$ with the mass of a Schwarzschild black hole, $M_s = \rho_s V_s$, where $\rho_s = M_s / \frac{4}{3}\pi r_s^3 \sim 10^{17} (M_\odot / M_s)^2 \text{ g cm}^{-3}$. From $M_{\text{rad}} \gtrsim M_s$, one finds that at cosmic time t , the mass of a possible Schwarzschild black hole would scale as [1]

$$M \gtrsim 10^{10} \text{ g} \frac{t}{10^{-29} \text{ s}}. \quad (2.1)$$

Coincidentally, this Schwarzschild black hole mass is comparable to the Hubble mass in a radiation-dominated era at cosmic time t [33, 36]

$$M_{\text{H}} = \frac{G}{2H} \sim 10^{10} \text{ g} \left(\frac{10^{11} \text{ GeV}}{T} \right)^2 \left(\frac{106.75}{g_*(T)} \right)^{1/2} \quad (2.2)$$

The above relation opens up a wide mass range for PBHs potentially formed in the early universe.

However, the fact that we do not observe a PBH zoo around us suggests that additional conditions must be satisfied for PBH formation. A widely studied mechanism proposes that PBHs form from primordial density fluctuations. These fluctuations are characterized by the density contrast, defined as

$$\Delta(x) \equiv \frac{\rho(x) - \bar{\rho}}{\bar{\rho}}, \quad (2.3)$$

where $\rho(x)$ is the local energy density on a space-like hypersurface and $\bar{\rho}$ is the cosmic average at a given instance. Early work by Carr and Hawking [37, 38] showed that an overdense region collapses into a PBH if its density contrast exceeds a threshold Δ_{min} , but remains below an upper bound Δ_{max} . The lower threshold, which is determined by the Jeans radius, ensures that the region can overcome its own pressure. The upper bound arises because a region with $\Delta > \Delta_{\text{max}}$ has a local geometry of its space-like hypersurface possessing a positive curvature, which is described by a compact and closed Friedmann universe. Unlike regions with $\Delta_{\text{max}} > \Delta > \Delta_{\text{min}}$, which collapse to form PBHs embedded in the background FRW universe, regions with $\Delta > \Delta_{\text{max}}$ evolve as self-contained universes because their geometry is compact and disconnected from the rest of spacetime.

More recent work has revisited these limits, with [39, 40] refining the estimates of Δ_{\max} , and [41] arguing that such estimates depend strongly on the selected geometry, which is not coordinate-invariant and may not impose robust constraints on physical density fluctuations. Therefore, we do not consider the scenario where $\Delta \gg \Delta_{\max}$ and the resulting acausal regions of spacetime.

A more reliable estimate for the lower threshold has been obtained through hydrodynamical simulations [42–45]. Through the examination of a spherical collapse model in a radiation fluid, these studies suggest that the PBH mass is related to the horizon mass at formation via a critical collapse, $M = K(\Delta - \Delta_c)^\gamma M_{\text{H}}$, where K , Δ_c , and γ are constants determined by specific simulation models. A representative set of values, $K = 11.9$, $\gamma = 0.34$, and $\Delta_c = 0.7015$ (Gaussian-curve perturbation), yields $M > 0.1M_{\text{H}}$ when $\Delta - \Delta_c$ only slightly exceeds 10^{-6} [43]. This framework provides a more accurate connection between density fluctuations and the expected PBH mass. While larger overdensities give rise to more massive PBHs, the lower threshold of the PBH mass can reasonably be identified with the horizon mass given in (2.2), or at least expected to lie within the same order of magnitude.

3 THE PRIMORDIAL BLACK HOLE MASS FRACTION

Having established that the characteristic PBH mass is comparable to the Hubble mass, we now evaluate the number of PBHs formed at a given epoch. The early universe can be divided into Hubble-sized regions of comoving scale $R = 1/aH$, where primordial inflationary fluctuations generate a density contrast $\Delta(x)$ defined in (2.3). Smoothing $\Delta(x)$ over the scale R with a window function W , $\Delta(x, R) = \int_{-\infty}^{\infty} d^3x' W(x-x', R)\Delta(x')$, assigns a single contrast value to each patch. Regions satisfying $\Delta \geq \Delta_c$ collapse into PBHs with masses $M \gtrsim M_{\text{H}}$.

References [35, 46] estimate the number density of peaks using the statistical approach introduced in [47], where the number of peaks follows $n_{\text{peaks}}(\nu > \nu_c) \propto \exp(-\nu_c^2/2)$, with $\nu_c^2 \equiv \Delta_c^2/\sigma_\Delta^2$. Here, Δ_c represents the threshold density contrast for collapse, and σ_Δ^2 is the variance of the smoothed density field, given by

$$\begin{aligned} \sigma_\Delta^2 &= \int_0^\infty \frac{dk}{k} W^2(k, R) \mathcal{P}_\Delta(k) \\ &= \int_0^\infty \frac{dk}{k} W^2(k, R) \frac{4(1+w)^2}{(5+3w)^2} (kR)^4 \mathcal{P}_{\mathcal{R}}(k). \end{aligned} \tag{3.1}$$

Here, $W(k, R)$ is the Fourier transformed window function. $\mathcal{P}_\Delta(k)$ and $\mathcal{P}_{\mathcal{R}}(k)$ denote the power spectrum of the smoothed density contrast and the primordial curvature perturbation, respectively. From [48], the curvature power spectrum is described by $\mathcal{P}_{\mathcal{R}} = A_{\mathcal{R}} (k/k_0)^{n_s-1}$, where $A_{\mathcal{R}} \approx 2.1 \times 10^{-9}$ is the amplitude of the scalar power spectrum, $n_s \approx 0.96$ is the scalar spectral index, and $k_0 = 0.05 \text{ Mpc}^{-1}$ is the pivot scale.

Physically, $n_{\text{peaks}}(\nu > \nu_c)$ represents the number of Hubble-sized patches that satisfy the collapse condition $\Delta \geq \Delta_c$, corresponding to the number of PBHs with $M \gtrsim M_{\text{H}}$ formed once overdense regions re-enter the horizon. Since the number density depends exponentially on Δ_c , PBHs with masses much larger than M_{H} are exponentially suppressed. For simplicity in our later analysis, we assume all PBHs form at the time of collapse with masses equal to the Hubble mass.

The PBH mass fraction is defined as $\beta(M) \equiv n(M) \times M/\rho$, where ρ is the background energy density. It can be expressed as

$$\beta = \frac{(n_s + 3)^{3/2}}{6^{3/2}(2\pi)^{1/2}} (\nu_c^2 - 1) e^{-\frac{\nu_c^2}{2}}, \quad (3.2)$$

In [35], authors relate β to the PBH mass $M \approx M_H$ by connecting the comoving scale R to the horizon mass through $M_H = M_{H,\text{eq}}(k_{\text{eq}}R)^2 (g_{*,\text{eq}}/g_*)^{1/3}$, where $g_{*,\text{eq}} \approx 3$, $k_{\text{eq}} = 0.07\Omega_m h^2 \text{Mpc}^{-1}$, $M_{H,\text{eq}} = 1.3 \times 10^{49}(\Omega_m h^2)^{-2} \text{g}$, and $\Omega_m h^2 = 0.14$. This mapping expresses the PBH mass in terms of comoving scale and cosmological parameters.

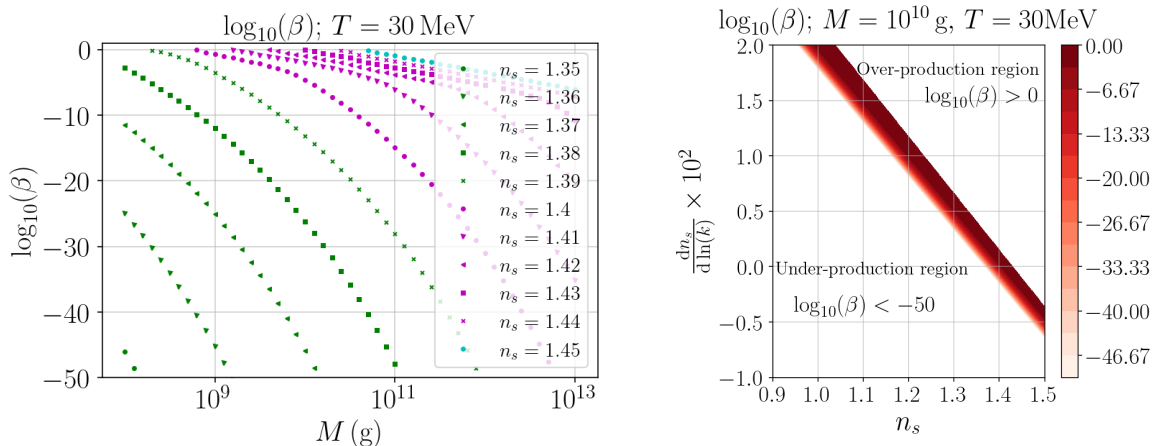


Figure 1. **Left:** PBH mass fraction β without a running n_s , from (3.2), at $T = 30 \text{ MeV}$, shown for different values of the scalar spectral index n_s . When $n_s < 1.38$, PBH formation is negligible ($\log_{10} \beta \lesssim -10$) within the relevant mass range. **Right:** Contour plot of the PBH mass fraction $\log_{10} \beta(M = 10^{10} \text{ g})$ as a function of n_s and its running $dn_s/d \ln(k)$ at $T = 30 \text{ MeV}$.

At horizon entry, PBHs behave as non-relativistic matter with $\rho_{\text{PBH}} \propto a^{-3}$, in contrast to radiation energy density, which redshifts as a^{-4} . Consequently, the PBH mass fraction $\beta(M)$ grows linearly with the scale factor a . If PBHs form at time t_i with an initial fraction $\beta_M(t_i)$, their fraction at a later time t_f evolves as

$$\beta_M(t_f) = \beta_M(t_i) \frac{a(t_f)}{a(t_i)}, \quad (3.3)$$

where the creation time t_i can be estimated using (2.1).

In the left panel of Fig. 1, we plot $\log_{10} \beta$ from (3.2) as a function of the PBH mass M . The considered mass range is $10^8 \text{ g} < M < 10^{13} \text{ g}$, since PBHs within this interval can influence BBN, as discussed later in Sec. 4. As an example, the first green square indicates that for $n_s = 1.38$, the mass fraction of PBHs with $M = 10^8 \text{ g}$ is $\beta \approx 10^{-2}$ at $T = 30 \text{ MeV}$. Only models with a scalar spectral index $n_s \geq 1.38$ yield a non-negligible PBH mass fraction ($\log_{10} \beta \gtrsim -10$) within the range relevant to our study. In contrast, the observed primordial power spectrum in the present universe is nearly scale-invariant, with $n_s \sim 1$, which explains why PBH contributions are not expected to be detectable through current BBN constraints.

Recent observations, however, allow for a scale-dependent scalar spectral index, commonly referred to as a *running* spectral index. It is parameterized by $n_s(k) = n_s + \frac{1}{2} \frac{dn_s}{d \ln(k)} \ln\left(\frac{k}{k_0}\right)$.

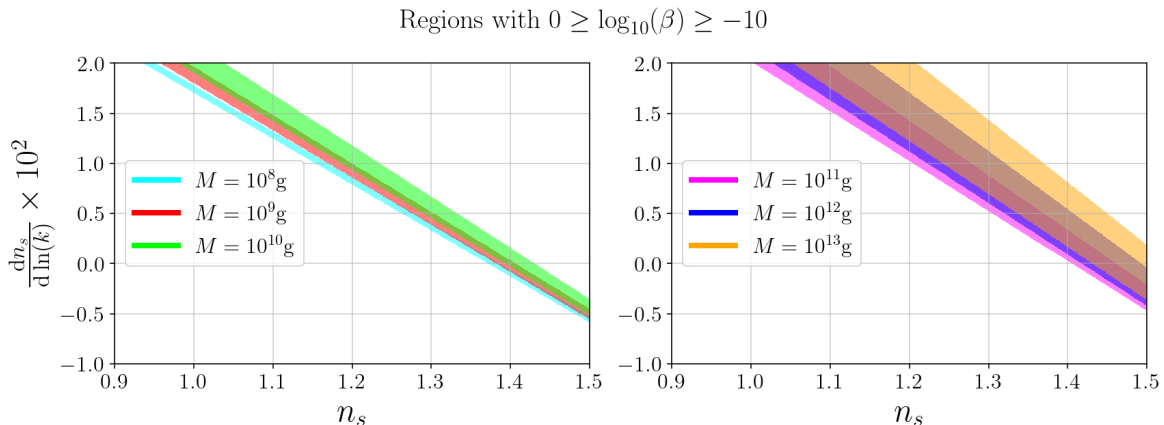


Figure 2. Contour plots showing regions of interest where $0 \geq \log_{10}(\beta) \geq -10$ for different PBH masses, evaluated at a cosmic temperature of $T = 30$ MeV. As the PBH mass increases, the region of interest broadens and shifts toward higher values of the scalar spectral index n_s . Heavier PBHs form more efficiently in spectra with larger n_s , consistent with the behavior observed in Fig. 1.

Current measurements [48] give $n_s = 0.9641 \pm 0.0044$ and $dn_s/d \ln(k) = -0.0045 \pm 0.0067$, evaluated at the pivot scale $k_0 = 0.05 \text{ Mpc}^{-1}$.

We now illustrate how the PBH mass fraction $\beta(M)$ varies with the scalar spectral index n_s and its running $dn_s/d \ln(k)$. As shown in the right panel of Fig. 1, for $M = 10^{10} \text{ g}$, $\log_{10} \beta$ exhibits a well-defined pattern in the $[n_s, dn_s/d \ln(k)]$ plane. The upper-right region corresponds to PBH overproduction ($\log_{10} \beta > 0$), while the lower-left region represents negligible PBH formation. Increasing $dn_s/d \ln(k)$ broadens the allowed range of n_s values for which PBHs can form. As shown in Fig. 2, this trend persists across PBHs of different masses: as M increases, the regions of interest satisfying $0 \geq \log_{10} \beta \geq -10$ become broader and shift toward larger n_s . This trend indicates that heavier PBHs form more efficiently in models with slightly higher spectral indices. Collectively, these figures demonstrate non-negligible PBH formation in the parameter space $[n_s, dn_s/d \ln(k)]$, providing the foundation for the subsequent analysis.

The introduction of a running spectral index opens the possibility of producing a significant PBH mass fraction even when n_s at CMB scales remains close to unity. To account for this effect in our calculation of $\beta(M)$, we replace the scale-invariant form of the spectrum with its running counterpart. Since no closed analytical expression for the variance (3.1) exists in this case, we rely on numerical evaluation using the BURST code [49, 50].

The BURST code, originally designed for BBN calculations, has been modified here to incorporate PBHs. A key improvement is its ability to compute a self-consistent scale factor $a(t)$, which is essential for accurately tracking the evolution of the PBH fraction in the universe. We begin by evaluating the PBH mass fraction, $\beta(M)$, at their formation time. This initial $\beta(M)$ depends on the parameters n_s , $dn_s/d \ln(k)$, and M . The obtained mass fraction is then evolved forward to the onset of the BBN era, beginning at a temperature $T = 30$ MeV.

After determining $\beta(M)$ at $T = 30$ MeV, we compute the emission of different particle species via Hawking radiation and track how this process alters $\beta(M)$ at each time step. The details of this calculation, including how Hawking radiation modifies the PBH mass fraction, will be discussed in Sec. 4.

Next, we incorporate the effect of Hawking evaporation on the background energy densities. Specifically, the radiation and matter energy densities are modified by including contributions from PBHs. Using Friedmann’s equations,

$$H(t)^2 = \frac{8\pi G}{3} \left[\frac{\rho_{\text{PBH}(t_i)} a^3(t_i)}{a^3(t)} + \frac{\rho_{\text{rad}(t_i)} a^4(t_i)}{a^4(t)} \right] \quad (3.4)$$

, we then evolve the scale factor $a(t)$. Because PBHs behave as non-relativistic matter, the ratio of $a(t)$ at the present time t_0 to its value at BBN time t_{BBN} is greater than in the standard ΛCDM model without PBHs. To ensure consistency, if $a(t_0)$ differs from unity by more than 10^{-6} , we iteratively adjust the initial estimate of $a(t_{\text{BBN}})$ until convergence is achieved.

4 CHANGE IN BBN FROM PBH DECAY

We have established both the physical conditions under which PBHs can form and the statistical framework that determines their expected mass fraction, β , at the onset of nucleosynthesis. With these ingredients in hand, we now turn to the central question of how the presence of PBHs modifies the dynamics of BBN. By emitting energetic particles through Hawking radiation, PBHs can inject entropy and alter reaction rates in the early plasma [26, 51, 52], thereby modifying the abundances of light elements relative to standard BBN predictions. Before addressing these modifications, it is useful to briefly recall the main features of standard BBN in the absence of PBHs.

In the standard scenario, BBN is modeled within a homogeneous and isotropic ΛCDM universe, together with the Standard Model of particle physics that includes three neutrino species. After inflation, the universe entered a radiation-dominated epoch during which reactions among elementary particles remained in equilibrium. As the universe cools to $T \approx 0.8\text{ MeV}$, the weak interaction rate governing neutron–proton conversions falls below the Hubble expansion rate, satisfying $\Gamma_{\text{W}} < H$ and marking the freeze-out of the neutron-to-proton ratio [53–55].

$n + e^+ \rightleftharpoons p + \bar{\nu}_e$	$n + \nu_e \rightleftharpoons p + e^-$	$n \rightleftharpoons p + e^- + \bar{\nu}_e$
--	--	--

Table 1. Weak reactions inter-converting neutrons to protons.

It is important to note, however, that the notion of a sharp “freeze-out” is only an approximation. Even after the weak interaction rate drops below the Hubble rate, neutron decay continues and lepton capture reactions still modify the neutron–proton ratio. As the universe cools further to $T \approx 0.1\text{ MeV}$, the photon background becomes dilute enough for deuterium to survive photodisintegration, despite its binding energy of 2.2 MeV . The small number of baryons per photon ($\eta \equiv n_{\text{b}}/n_{\gamma}$) delays this process until relatively low temperatures, but once it occurs, light nuclei can form and persist.

Because of the Coulomb barrier, the synthesis of nuclei beyond $A = 8$ is strongly suppressed, leaving only trace amounts of heavier elements (e.g., ${}^9\text{Be}$, ${}^{10}\text{B}$). As a result, the observable relics of BBN are ${}^1\text{H}$, D , ${}^3\text{He}$, ${}^4\text{He}$, also with ${}^6\text{Li}$ and ${}^7\text{Li}$ produced at much lower levels. The primordial abundance of ${}^6\text{Li}$ remains uncertain because it is readily destroyed in stellar environments, whereas ${}^7\text{Li}$ is consistently overproduced in standard BBN compared with observational data — a long-standing discrepancy known as the “lithium problem” [56–58]. Comparisons between the observed and predicted primordial abundances of these light

elements provide valuable insights into the physics of the early universe. In this work, we will focus on ^4He , D, ^3He , and ^7Li .

In standard BBN, nearly all free neutrons are incorporated into ^4He . Consequently, the primordial ^4He abundance is determined primarily by the neutron-to-proton ratio prior to nucleosynthesis. This ratio can be approximated by the Boltzmann factor $n/p \approx e^{-\Delta m/T_f} \approx 1/5$, where $\Delta m = m_n - m_p$ and $T_f \approx 0.8\text{ MeV}$ is the freeze-out temperature [59]. Below this temperature, weak interactions involving free neutron decay and lepton capture processes continue to reduce the ratio to $n/p \approx 1/7$, yielding a helium mass fraction of $Y_P = n(^4\text{He})m(^4\text{He})/n_b m_b = 2(n/p)/[1 + (n/p)] \approx 0.25$. Observational determinations of ^4He from emission lines in H-II regions suggest $Y_P = 0.2345 \pm 0.0026$ [60], while more recent analyses using Markov Chain Monte Carlo techniques yield $Y_P = 0.2449 \pm 0.0040$ [61].

Although the freeze-out estimate provides useful intuition, it is only approximate and neglects important nuclear processes. Given the precision of modern observations of Y_P , reliable predictions require following the full weak and nuclear reaction network rather than relying on such simplified arguments. This is particularly relevant for understanding the nontrivial variations of Y_P that emerge in our analysis of PBH effects in Sec. 5.2.

Among the light elements, deuterium (D) is particularly valuable as a probe of the baryon-to-photon ratio, since the deuterium-to-hydrogen ratio (D/H) decreases monotonically with η and is highly sensitive to it [62, 63]. A higher baryon density allows nuclear reactions to proceed more efficiently, synthesizing nearly all of the deuterium into helium. Moreover, D/H can be directly measured from absorption spectra in metal-poor, damped Lyman- α systems. Recent observations report $\text{D}/\text{H} = (2.527 \pm 0.030) \times 10^{-5}$ [64]. ^3He provides another sensitive indicator of η , though its interpretation is complicated by continuous production and destruction in stellar environments [65]. As a result, present-day measurements of ^3He are less robust indicators of η than deuterium. Measurements in Galactic H-II regions yield $^3\text{He}/\text{H} = (1.1 \pm 0.2) \times 10^{-5}$ [66]. ^7Li remains the most puzzling case: standard BBN, calibrated by the baryon density inferred from CMB data, predicts abundances significantly higher than those observed in metal-poor halo stars, where $^7\text{Li}/\text{H} = (1.23^{+0.68}_{-0.32}) \times 10^{-10}$ [67, 68].

Having outlined the key features of standard BBN, we now turn to how this picture is modified in the presence of PBHs. PBHs can influence BBN in several ways, but one of the crucial effects arises from Hawking radiation, through which they inject high-energy particles into the primordial plasma. A black hole of mass M radiates particles at a characteristic temperature [69]

$$T_{\text{BH}} = \frac{1}{8\pi GM} \approx 10^6 (10^{10} \text{ g}/M) \text{ MeV}. \quad (4.1)$$

Any Standard Model particle with energy below this temperature can be emitted. While the precise energy of an emitted particle depends on its species, it is sufficient for our purposes to approximate the emission energy as $E \approx T_{\text{BH}}$.

Hawking radiation causes the black hole to lose mass at a rate [70]

$$\frac{dM}{dt} = -5.34 \times 10^{25} f(M) (1 \text{ g}/M)^2 \text{ g sec}^{-1}, \quad (4.2)$$

where $f(M)$ encodes the number of particle species emitted and is normalized to unity when $M \gg 10^{17} \text{ g}$. This formulation, introduced in studies of quark-gluon jet emission, provides the basis for estimating PBH evaporation timescales.

Integrating this expression yields the black hole lifetime,

$$\tau_{\text{BH}} \approx 6.24 \times 10^{-27} (M/1 \text{ g})^3 f(M)^{-1} \text{ sec} \approx 1.98 \times 10^{-34} (M/1 \text{ g})^3 f(M)^{-1} \text{ yr}. \quad (4.3)$$

For example, with $M = 10^{13} \text{ g}$ and $f(M) \approx 12.5$, the lifetime is $\tau_{\text{BH}} \sim 5 \times 10^{11} \text{ s} \approx 1.6 \times 10^4 \text{ yr}$. A PBH of mass 10^{15} g instead survives for $\tau_{\text{BH}} \sim 10^{10} \text{ yr}$, comparable to the current age of the universe.

The function $f(M)$ accounts for the evaporation rates of different particle species, including leptons l , quarks q , neutrinos a , gluons g , W and Z bosons, as well as the Higgs boson. Its explicit form, incorporating spin-dependent weights and degrees of freedom, is given by [71]

$$\begin{aligned} f(M) = & 2f_1 + 4f_{1/2}^1 \left[\sum_{l=e,\mu,\tau} \exp\left(-\frac{M}{s_{1/2}M_l}\right) + 3 \sum_q \exp\left(-\frac{M}{s_{1/2}M_q}\right) \right] \\ & + 2\eta_\nu^N f_{1/2}^0 \sum_{a=1,2,3} \exp\left(-\frac{M}{s_{1/2}M_a}\right) \\ & + 16f_1 \exp\left(-\frac{M}{s_1M_g}\right) \\ & + 3f_1 \left[2 \exp\left(-\frac{M}{s_1M_W}\right) + \exp\left(-\frac{M}{s_1M_Z}\right) \right] + f_0 \exp\left(-\frac{M}{s_0M_{\text{Higgs}}}\right), \end{aligned} \quad (4.4)$$

where $M_j = 1/(8\pi Gm_j)$ corresponds to the PBH mass whose Hawking temperature equals the rest mass m_j of a given particle species. Massless photons contribute to the first term, $2f_1$, while massless gluons are assigned an effective mass $m_g = 0.6 \text{ GeV}$, corresponding to the infrared cutoff in QCD renormalization [72]. The coefficients s_s, f_s^q , and η_ν^N encode the spin and charge dependent parameters, and distinguish between Dirac and Majorana neutrinos. Their numerical values are summarized in

$$\begin{aligned} s_0 &= 2.66, \quad s_{1/2} = 4.53, \quad s_1 = 6.04 \\ f_0 &= 0.267, \quad f_1 = 0.060 \\ f_{1/2}^0 &= 0.147 \text{ (uncharged)}, \quad f_{1/2}^1 = 0.142 \text{ (charged)} \\ \eta_\nu^{\text{Dirac}} &= 2, \quad \eta_\nu^{\text{Majorana}} = 1. \end{aligned} \quad (4.5)$$

While PBHs emit the full spectrum of Standard Model particles, not all of them propagate freely into the cosmological plasma. Whether an emitted particle significantly affects the background depends on its mean free path relative to the black hole's characteristic and inter-separation scale. This criterion is key to identifying which emissions influence BBN and may lead to inhomogeneous heating during BBN. Previous studies [51] examined PBHs with masses in the range $10^9 \text{ g} \leq M \leq 10^{12} \text{ g}$, and found that only photons, with mean free path $l_\gamma \sim 10^{-9} \text{ cm}$, and neutrinos, with $l_\nu \sim 10^{-11} \text{ cm}$ travel farther than the Schwarzschild radius of a PBH with $M \sim 10^{10} \text{ g}$ ($r_s \sim 10^{-17} \text{ cm}$). The vicinity of a black hole would therefore be transparent only to photons and neutrinos, which can directly participate in background nuclear reactions (see Tab. 1 and 2).

For heavier particles, the mean free path is much smaller, and therefore annihilate quickly around a cloud of PBH's horizon size [51]. Within our approximation, ignoring inhomogeneous heating during BBN is justified. Previous works [73, 74] have therefore suggested

that evaporating PBHs do not release such species as free-streaming particles. Instead, their emissions thermalize within an optically thick “hot envelope” surrounding the PBHs. High-energy particles undergo repeated scatterings with the background plasma, quickly reaching a new thermal equilibrium. A similar treatment of rapid thermalization of PBH emissions is used in [26]. Following this picture, we assume that massive particles influence BBN only indirectly: by depositing their energy into the surrounding medium, they heat the plasma and contribute to its entropy density. While we do not consider the direct interaction of injected hadrons/mesons with the background plasma, complementary analyses based on different assumptions instead track the hadronic/meson component explicitly and study its effect on the neutron-to-proton conversion rate [25].

In the BURST calculations, we first scan a parameter space spanned by the scalar spectral index n_s , its running $dn_s/d\ln(k)$, and the PBH mass M . To ensure that the universe remains radiation-dominated at the onset of nuclear reactions, we impose the condition that the PBH mass fraction at $T = 30$ MeV satisfies $\beta(n_s, dn_s/d\ln(k), M) \leq 1$. The scalar spectral index is varied within $0.9 \leq n_s \leq 1.5$, while the running is constrained to $-0.010 \leq dn_s/d\ln(k) \leq 0.020$. For the PBH mass, we consider the range $10^8 \text{ g} \leq M \leq 10^{13} \text{ g}$. The lower bound reflects the fact that PBHs lighter than 10^8 g evaporate completely before BBN, while the upper bound corresponds to $\tau \approx 5 \times 10^{11} \text{ s}$, such that evaporation ends well before observables like the CMB are affected.

Once a viable combination $\beta(n_s, dn_s/d\ln(k), M)$ is identified, it is incorporated into the BBN reaction network. In our framework, PBHs primarily act as sources emitting neutrinos and plasma particles through Hawking radiation. At high temperatures, before photons and neutrinos decouple (when neutrino–electron and neutrino–positron weak interactions remain efficient), all species share a common temperature governed by local thermal equilibrium. As the universe cools and photons and neutrinos decouple (at an equivalent of $T_{\text{dec}} \approx 1.5$ MeV in the absence of PBHs [75]), the neutrino and plasma sectors evolve separately. We make the assumption that neutrinos remain in Fermi–Dirac equilibrium with zero chemical potential, thereby neglecting energy down-scattering transport processes. Reference [50] gives the prescription for evolving the temperature under such constraints. Meanwhile, the plasma particles continue to thermalize through Compton scattering, double Compton scattering, and bremsstrahlung. The non-neutrino energy density emitted by PBHs are assumed to instantaneously thermalize with the surrounding plasma, injecting entropy into the background, while the emitted neutrinos directly participate in background weak and nuclear reactions.

${}^1_1\text{H}(n, \gamma){}^2_1\text{H}$	${}^2_1\text{H}(n, \gamma){}^3_1\text{H}$	${}^3_2\text{He}(n, \gamma){}^4_2\text{He}$	${}^6_3\text{Li}(n, \gamma){}^7_3\text{Li}$
${}^3_2\text{He}(n, p){}^3_1\text{H}$	${}^7_4\text{Be}(n, p){}^7_3\text{Li}$	${}^6_3\text{Li}(n, \alpha){}^3_1\text{H}$	${}^7_4\text{Be}(n, \alpha){}^4_2\text{He}$
${}^2_1\text{H}(p, \gamma){}^3_2\text{He}$	${}^3_1\text{H}(p, \gamma){}^4_2\text{He}$	${}^6_3\text{Li}(p, \gamma){}^7_4\text{Be}$	${}^6_3\text{Li}(p, \alpha){}^3_2\text{He}$
${}^7_3\text{Li}(p, \alpha){}^4_2\text{He}$	${}^2_1\text{H}(\alpha, \gamma){}^6_3\text{Li}$	${}^3_1\text{H}(\alpha, \gamma){}^7_3\text{Li}$	${}^3_2\text{He}(\alpha, \gamma){}^7_4\text{Be}$
${}^2_1\text{H}({}^2_1\text{H}, n){}^3_2\text{He}$	${}^2_1\text{H}({}^2_1\text{H}, p){}^3_1\text{H}$	${}^3_1\text{H}({}^2_1\text{H}, n){}^4_2\text{He}$	${}^3_2\text{He}({}^2_1\text{H}, p){}^4_2\text{He}$
${}^3_2\text{He}({}^3_2\text{He}, 2p){}^4_2\text{He}$	${}^7_3\text{Li}({}^2_1\text{H}, n\alpha){}^4_2\text{He}$	${}^7_4\text{Be}({}^2_1\text{H}, p\alpha){}^4_2\text{He}$	

Table 2. Nuclear reaction chain in the BURST code [49, 50].

Because PBHs increase the comoving entropy density through Hawking radiation, we adjust the initial baryon-to-photon ratio η at $T = 30$ MeV to a greater value than in standard BBN. This adjustment ensures that the final baryon-to-photon ratio at $T = 8.6 \times 10^{-4} \text{ keV} \approx 10^4 \text{ K}$ matches the observed CMB value of $\eta = 6.1 \times 10^{-10}$ [48]. Practically, we determine

a self-consistent η by an iterative correction procedure analogous to that used for the scale factor $a(t)$ in Sec. 3: we evolve the system with an initial guess for η , compare the resulting value with the target, and repeat until the relative difference falls below 10^{-6} . This yields consistent values of $a(t)$ and η that fully incorporate both the PBH mass fraction and entropy injection from Hawking radiation.

With the PBH model $\beta(n_s, dn_s/d\ln(k), M)$ and the corresponding initial conditions, we evolve the full nuclear reaction network forward in time, including all processes listed in Tables 1 and 2. At each timestep, the PBH mass-loss rate is computed using (4.2) and (4.4), and the associated energy transfer to the plasma is tracked as a continuous heating source. PBH photons and neutrinos, owing to their long mean free paths, deposit their energy directly into the corresponding plasma, while heavier PBH decay products heat the plasma indirectly through secondary interactions confined in the hot envelope. This energy injection modifies the background photon and neutrino temperatures, as well as the neutrino number density, thereby influencing both the weak and nuclear reaction rates and the Hubble expansion rate. In this way, PBH evaporation affects the thermal history and the nuclear processes of BBN, providing the physical basis for the results discussed in the next section.

5 RESULTS

5.1 Entropy and Primordial Abundances

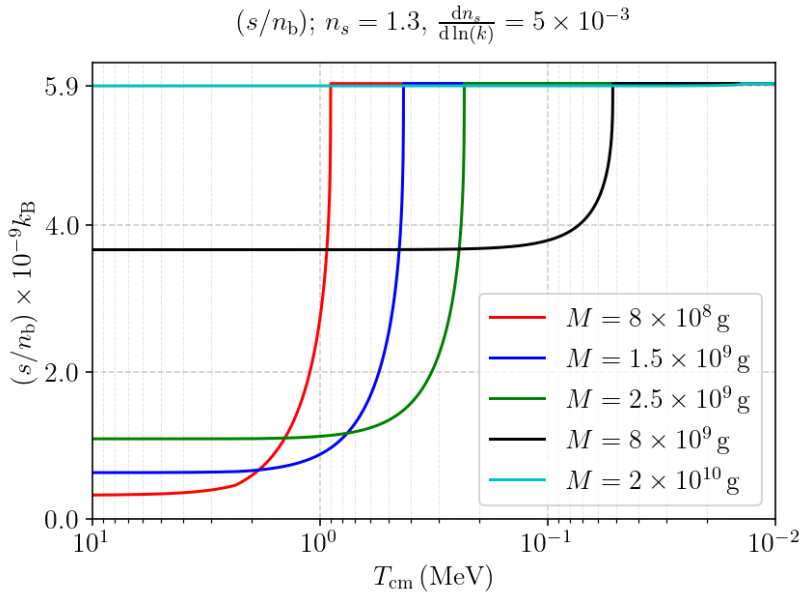


Figure 3. Evolution of the comoving entropy density per baryon, (s/n_b) as a function of comoving temperature quantity, T_{cm} , in the case $n_s = 1.3$ and $dn_s/d\ln(k) = 5 \times 10^{-3}$. Each curve represents a different mass and would have a different initial value of β .

Here we present the key findings of our calculations: the comoving entropy density increases as the universe expands and cools during the nucleosynthesis epoch. Previous studies constraining the PBH fraction using BBN generally neglected entropy variation, since they considered only extremely small PBH abundances ($\beta(M) \sim 10^{-20}$) [32, 33, 76], for which particle emission has a negligible effect on plasma heating. In contrast, our framework allows for

($\beta(M) \sim 1$), where PBH evaporation significantly alters the comoving entropy density, making it essential to account for this variation to ensure a self-consistent cosmological evolution in our PBH-BBN simulations.

Figure 3 shows the evolution of the comoving entropy density per baryon s/n_b as a function of decreasing comoving temperature. We consider a single value of the spectral index and the running, although the results in this figure generalize to other $[n_s, dn_s/d\ln(k)]$ pairs. Each curve represents a different PBH mass. For models with negligible PBH effects (cyan curve with $M = 2 \times 10^{10}$ g), the evolution nearly reproduces the standard cosmology: the comoving baryon number and entropy densities remain conserved after baryogenesis, yielding the present-day values $(s/n_b) = 5.9 \times 10^9 k_B$. When PBH evaporation becomes significant, entropy injection from Hawking radiation increases (s/n_b) . To reproduce the observed CMB value at late times, the universe must begin with a lower initial entropy density. The discontinuity in the slope of each curve marks the event of complete PBH evaporation corresponding to its mass.

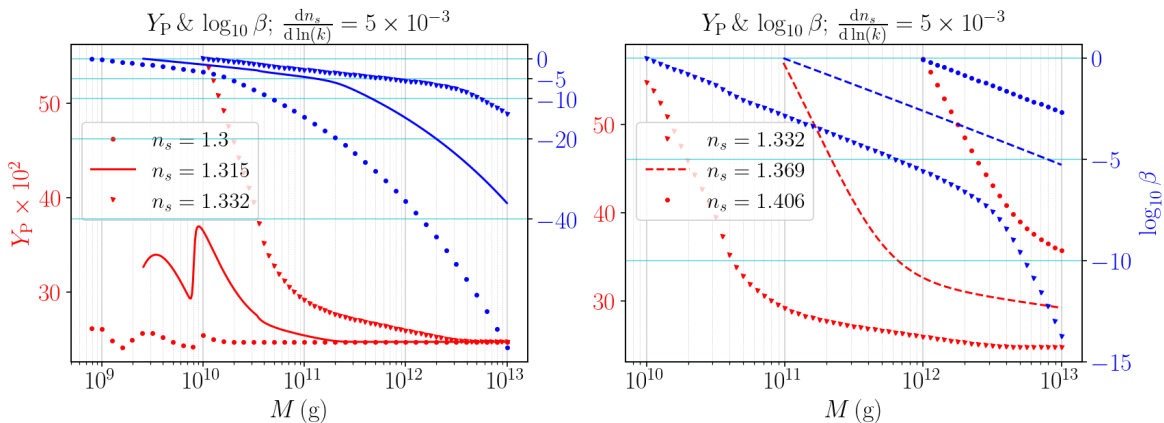


Figure 4. Mass fraction of ${}^4\text{He}$ (Y_P , red, left axis) and the PBH mass fraction ($\log_{10} \beta$ at $T = 30$ MeV, blue, right axis) as functions of PBH mass M for multiple values of n_s and $dn_s/d\ln(k) = 5 \times 10^{-3}$.

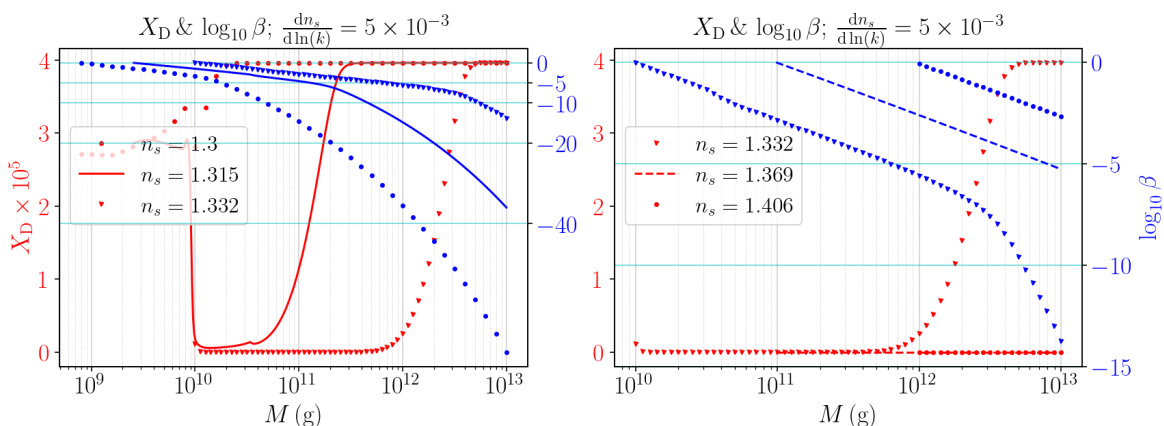


Figure 5. Same as Fig. 4 but for the deuterium mass fraction X_D .

We note that the lower-mass models ($M < 10^{10}$ g) in Fig. 3 completely evaporate

when the background comoving temperature T_{cm} falls between 1 MeV and 0.1 MeV. This temperature range is particularly important as it coincides with the epoch when light-element abundances depart from nuclear statistical equilibrium as the nuclear reaction rates fall below the Hubble expansion rate. Consequently, the $M \sim 10^{10}$ g value presents a transition region where complete PBH evaporation occurs before/after out-of-equilibrium nucleosynthesis.

We give the primordial abundance results for our $[n_s, dn_s/d\ln(k), M]$ extended PBH-BBN models. Figures 4, 5, 6, and 7 show the primordial abundances of Y_{P} , X_{D} , $X_{^3\text{He}}$, and $X_{^7\text{Li}}$, respectively, as red symbols over a range of masses and spectral indices. The right panel of each figure focuses on the mass range above the $M \sim 10^{10}$ g threshold, whereas the left figure includes masses below the threshold. In addition, we plot the value of β as blue symbols for each corresponding PBH model. As an example, the first red triangle in both panels of Fig. 4 corresponds to a PBH model with $n_s = 1.332$, $dn_s/d\ln(k) = 5 \times 10^{-3}$, and $M = 10^{10}$ g. Our BURST code calculation shows that this PBH model yields $\beta \approx 1$ (at the start of the BURST run at $T = 30$ MeV) and ^4He mass fraction, $Y_{\text{P}} \approx 55\%$.

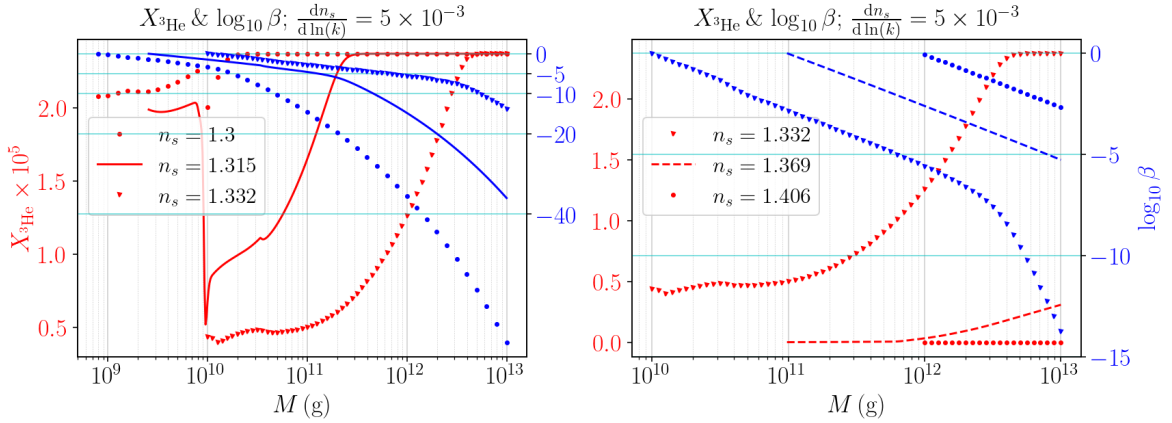


Figure 6. Same as Fig. 4 but for the ^3He mass fraction $X_{^3\text{He}}$.

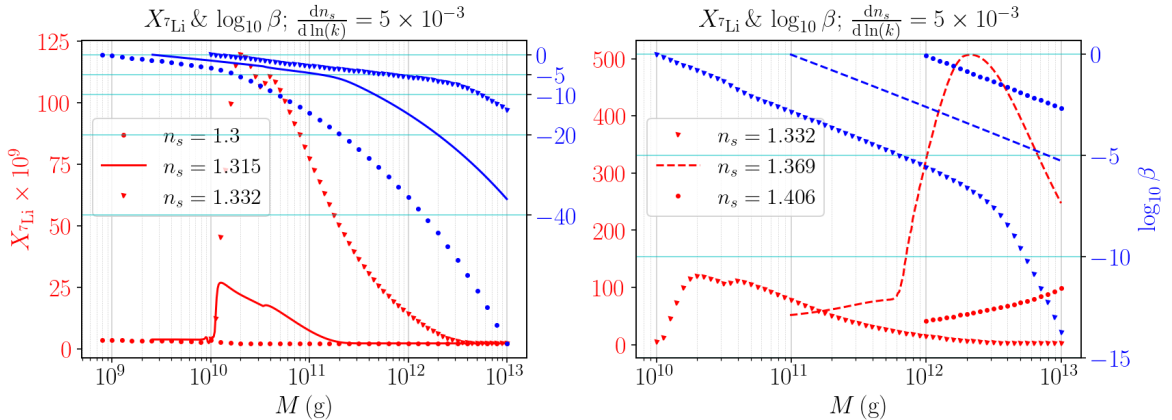


Figure 7. Same as Fig. 4 but for the ^7Li mass fraction $X_{^7\text{Li}}$.

In each plot from Fig. 4 to 7, we observe that when the PBH mass fraction satisfies $\beta < 10^{-10}$, the presence of PBHs has a negligible impact on the light element abundances

because of their very small fraction. In this regime, the abundances converge to values consistent with a standard computation of BBN absent PBHs. Those predicted primordial abundances are consistent with the observed values, except for $X_{7\text{Li}}$, which remains roughly a factor of 5 higher than the observed value [56, 57].

These four figures reveal a clear change in behavior of light element abundances around $M \approx 10^{10}$ g, indicating that PBHs with $M < 10^{10}$ g and those with $M > 10^{10}$ g influence BBN through different mechanisms. For $M < 10^{10}$ g, Y_{P} shows an oscillatory dependence on PBH mass, while the deuterium abundance, X_{D} , and the helium-3 abundance, $X_{3\text{He}}$, are slightly suppressed in the presence of PBHs. In this region, the lithium-7 abundance, $X_{7\text{Li}}$, experiences a modest enhancement.

For $M > 10^{10}$ g, Y_{P} increases monotonically as a function of β , largely independent of PBH mass. Both X_{D} and $X_{3\text{He}}$ are strongly suppressed at large β , regardless of M . In contrast, $X_{7\text{Li}}$ does not follow a similar pattern: its maximum variation does not occur at the largest β . Instead, the peak in the $n_s = 1.332$ curve appears at $\log_{10}(\beta) \approx -2$, while the peak in the $n_s = 1.369$ curve occurs at $\log_{10}(\beta) \approx -4$. Overall, in the region $M > 10^{10}$ g, the light element abundances are more strongly correlated with the PBH mass fraction β than with the PBH mass M .

The net contribution of PBHs with mass M to light element abundances is complex. Nevertheless, it can be decomposed into three main components: (i) high-energy photons from Hawking radiation, (ii) high-energy neutrinos from Hawking radiation, and (iii) modification of the Hubble rate due to the presence of PBHs.

The injection of high-energy photons through Hawking radiation heats the background photons, which are tightly coupled to baryons before decoupling. As a result, the average kinetic energy of all particle species in thermal equilibrium increases. The increased energy of charged particles raises the tunneling probability through the Coulomb barrier, further amplifying reaction rates. On the other hand, a hotter photon bath strengthens photodisintegration processes, which counteract nuclear synthesis. The larger net rates result in keeping the light-element abundances closer to nuclear statistical equilibrium [77].

Similarly, the injection of high-energy neutrinos via Hawking radiation heats the background neutrino bath, enhancing reaction rates involving neutrinos. An increased neutrino number density also shifts the reactions inter-converting protons and neutrons (see Tab. 1) to a new weak equilibrium, thereby modifying the neutron-to-proton ratio n/p .

Finally, if a significant fraction of PBHs remains during BBN, they substantially increase the Hubble rate $H(t)$. A higher expansion rate shortens the effective duration of BBN, precipitating an earlier nuclear freeze-out when reaction rates drop below the Hubble rate.

5.2 Distinct BBN Behavior Across the Threshold

To determine the origin of the $M \sim 10^{10}$ g threshold for the primordial abundance patterns in Figs. 4 – 7, we will consider an argument based on weak freeze-out, i.e., the period of BBN when the processes in Tab. 1 fall below the Hubble expansion rate. Although this is a protracted epoch, we will utilize an instantaneous “freeze-out temperature” T_{fo} for simplicity. How T_{fo} changes with β will allow us to focus on the relationship between energy density and the primordial abundances while temporarily ignoring changes from the injection of entropy.

To wit, we will suppose a typical weak interaction rate scales as $\Gamma_{\text{w}} \sim T^5$. In matter-dominated conditions, the Hubble expansion rate scales as $H \sim \sqrt{\beta T^3}$. Equating the two rates at freeze-out yields

$$T_{\text{fo}} \sim \beta^{1/7}. \quad (5.1)$$

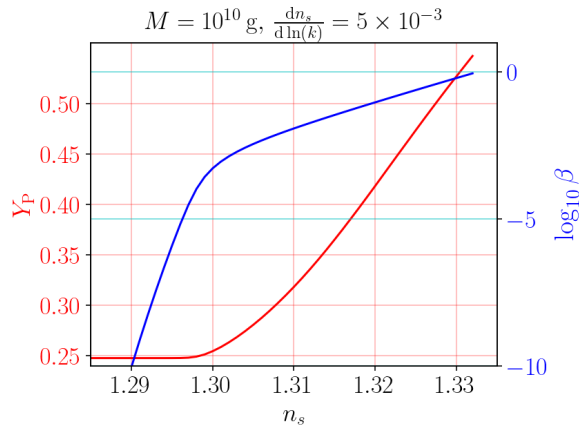


Figure 8. Y_{P} (red) and $\log_{10} \beta$ (red) plotted against n_s for $dn_s/d \ln(k) = 5 \times 10^{-3}$.

As β increases, we expect an earlier freeze-out epoch which leads to larger n/p and hence a larger Y_{P} .

Figure 8 exhibits the expected qualitative behavior for $M = 10^{10}$ g. We increase β (blue curve) by increasing the spectral index while keeping the running constant. As β increases from negligible values to the dominant energy component, Y_{P} (red curve) increases from the baseline value to above 0.5. We surmise that the freeze-out approximation is consistent with the changes in Y_{P} for $M \gtrsim 10^{10}$ g.

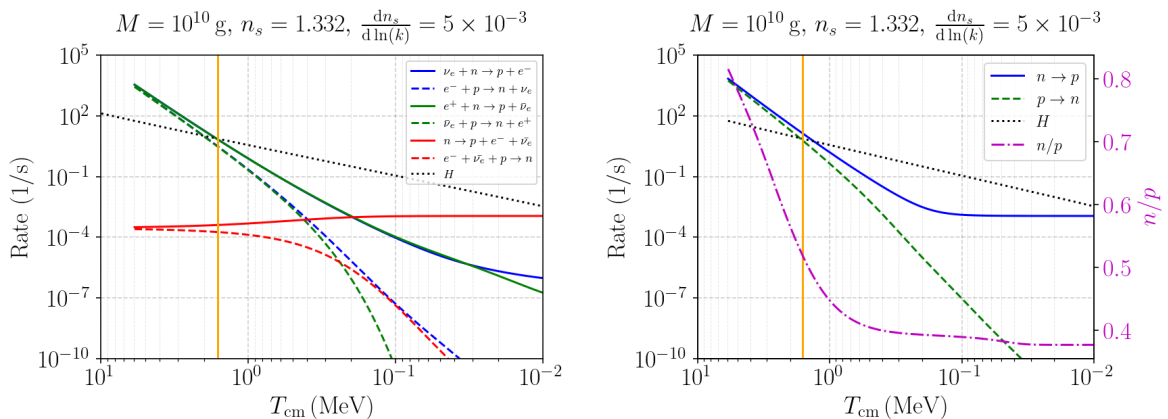


Figure 9. Left: Reaction rates from Table 1 and the Hubble expansion rate as functions of the comoving temperature T_{cm} for a model where $M = 10^{10}$ g, $n_s = 1.332$, and $dn_s/d \ln(k) = 5 \times 10^{-3}$. The orange vertical line gives the epoch when the net neutron destruction rate is equal to the Hubble expansion rate. **Right:** All forward reactions ($n \rightarrow p$ in left panel) summed into the solid blue line, and all backward reactions ($p \rightarrow n$) summed into the green dashed line. Also included is the Hubble expansion rate, and n/p .

Before we consider the mass range $M \lesssim 10^{10}$ g, we give more details on the neutron-to-proton interconversion rates in the presence of PBHs. In Fig. 9, we plot neutron-to-proton reaction rates, the Hubble expansion rate, and the neutron-to-proton ratio. The left panel gives the three neutron destruction rates (solid lines), three neutron creation rates (dashed lines), and the Hubble expansion rate for $M = 10^{10}$ g, $n_s = 1.332$, and $dn_s/d \ln(k) = 5 \times 10^{-3}$.

As seen in Fig. 4, these parameter values correspond to a model where β is nearly 1. This pushes T_{fo} (orange vertical line) to an earlier epoch. The right panel of Fig. 9 includes the evolution of n/p , along with summed forward and reverse neutron-to-proton rates and the Hubble expansion rate. The early epoch of weak freeze-out leads to the larger asymptotic value of n/p .

Figure 10 includes the right panel of Fig. 9 [panel (a)] along with 3 other mass values $M > 10^{10}$ g. As the mass increases, β decreases, as evidenced by the lowering of the dotted black line in panels (a) through (d). The decrease in β pushes T_{fo} to lower temperatures. For $M = 10^{12}$ g, β has dropped to 10^{-6} and the evolution of n/p aligns with standard BBN. Figures 8 and 10 are consistent with the precept that the n/p and the primordial abundances change in accordance to a changing Hubble expansion rate.

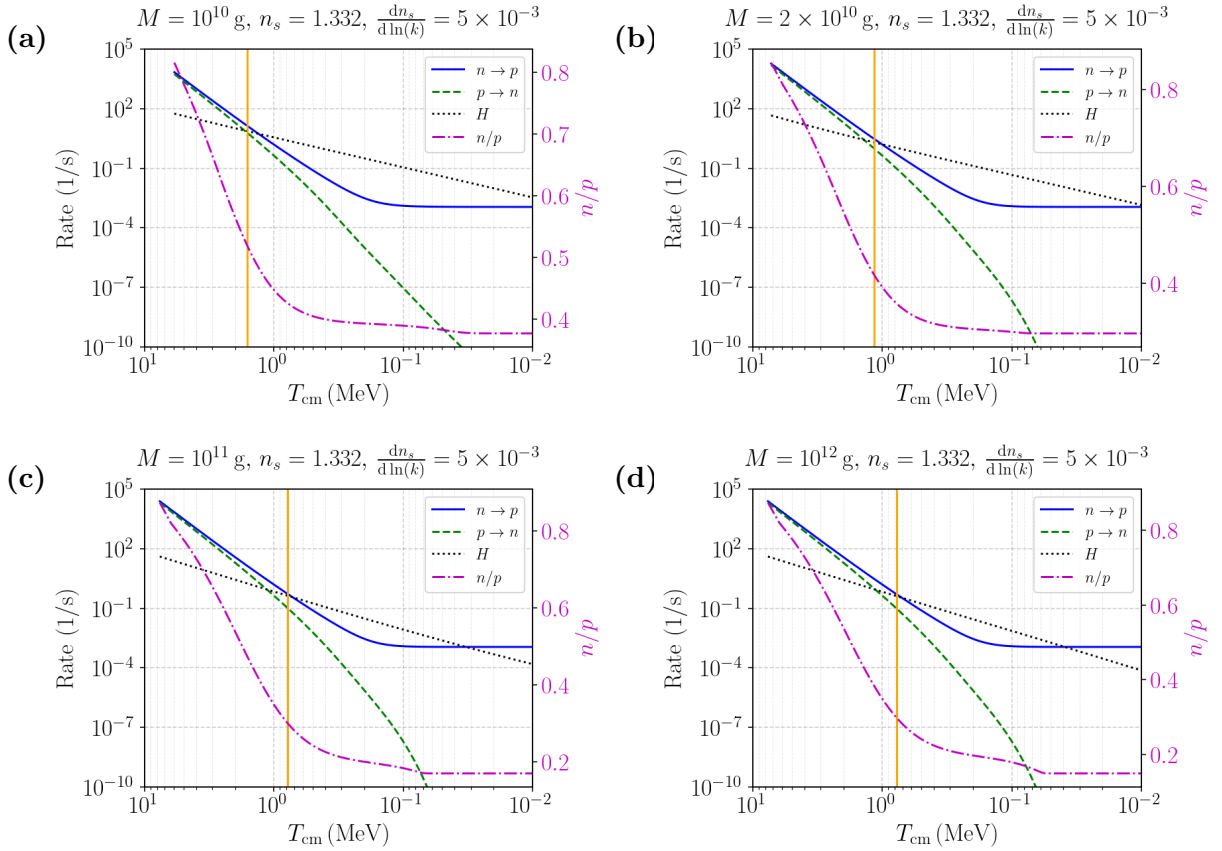


Figure 10. Same as the the right panel of Fig. 9 for a model where $n_s = 1.332$, and $dn_s/d\ln(k) = 5 \times 10^{-3}$. Each panel corresponds to a different mass, ranging from 10^{10} to 10^{12} g.

As emphasized in Sec. 5.1, PBHs with $M < 10^{10}$ g can completely evaporate during BBN, altering the thermal and nuclear dynamics. This behavior is illustrated in Fig. 11, which shows how PBH evaporation modifies the evolution of the reaction rates and the Hubble rate. As in Fig. 11, β decreases with increasing mass in panels (a) through (d). The cusps readily apparent in the neutron-to-proton rates and n/p (yet clearly absent in H) reflect the epoch when the PBHs cease to exist. Heavier PBHs possess longer lifetimes, so evaporation cusps appear at progressively lower temperatures. However, we notice that T_{fo} does not follow the same monotonic trend as Fig. 10, with T_{fo} increasing by nearly a factor

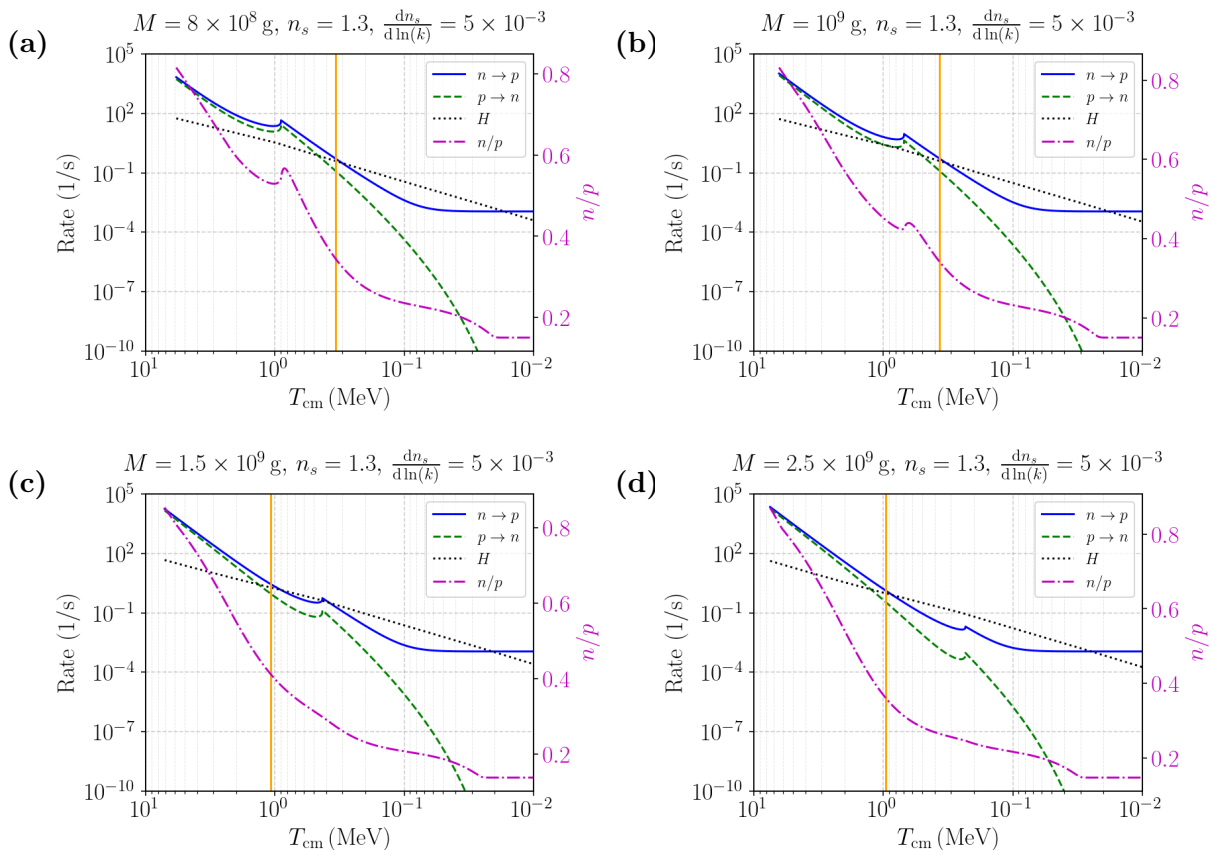


Figure 11. Same as Fig. 10 for a model where $n_s = 1.3$, and $dn_s/d\ln(k) = 5 \times 10^{-3}$. Each panel corresponds to a different mass, ranging from 8×10^8 to 2.5×10^9 g.

of 3 between panels (b) and (c). Here, the entropy injection is of paramount importance. The relationship between n/p and increasing entropy cannot be so easily dissected for these lower masses.

The conventional neutron freeze-out picture, in which a higher n/p ratio always yields a larger Y_P , breaks down in the low-mass regime. For example, panel (a) of Fig. 11 gives $n/p < 0.4$ at the freeze-out temperature, while panel (c) yields $n/p \gtrsim 0.4$. However, panel (a) corresponds to the first peak in the Y_P curve of Fig. 4, which is higher than the first valley associated with panel (c). This complex behavior arises from the interplay between the PBH lifetime (which sets the timing of evaporation) and the PBH mass fraction β (which determines whether evaporation can momentarily enhance reaction rates above H). As a result, for $M \leq 10^{10}$ g, evaporation induces an oscillatory pattern in Y_P , indicating that a more detailed treatment is needed to generalize this analysis to other light elements.

6 SUMMARY AND CONCLUSION

We investigated the role of PBHs in BBN based on mean free path arguments. In this picture, photons and neutrinos emitted by PBHs can propagate into the cosmological plasma and participate directly in background nuclear reactions, while heavier particles thermalize within a thick hot envelope surrounding the PBHs, transferring their energy to the plasma and

increasing its entropy. As a function of $n_s, dn_s/d\ln(k)$, and M , we construct dual PBH-BBN models in the BURST code by self-consistently coupling the Hubble expansion rate, entropy density, neutrino heating, and nuclear reaction network together to predict primordial nuclide abundances.

We again stress the key outcome of our analysis: PBH evaporation will substantially increase the comoving entropy density. Previous studies focused on relatively small PBH mass fractions ($\beta \sim 10^{-20}$) and neglected the plasma heating from Hawking radiation, while more recent analyses incorporate the entropy injection explicitly [26]. In the presence of a larger PBH mass fraction, Fig. 3 clearly shows the magnitude and epoch of the entropy increase from PBH evaporation. Furthermore, the neutrino component of the Hawking radiation changes the neutron-to-proton interconversion rates as demonstrated in Figs. 9 – 11. Coupled together, the non-standard evolution of the entropy and neutrino densities induce the novel primordial abundance patterns visible in Figs. 4 – 7, none of which follow from simple scaling laws over the PBH mass range we study. Our findings highlight the necessity of incorporating entropy evolution self-consistently when modeling the gravitational and nuclear physics of PBH-BBN interactions.

Our results (in Fig. 4 – 7) reveal a threshold near $M \approx 10^{10}$ g that separates two distinct regimes of BBN behavior. For $M \leq 10^{10}$ g, Y_{P} exhibits oscillatory dependence on PBH mass, while X_{D} and $X_{3\text{He}}$ are slightly suppressed, and $X_{7\text{Li}}$ shows modest enhancement. For $M > 10^{10}$ g, Y_{P} increases monotonically with β , with X_{D} and $X_{3\text{He}}$ strongly suppressed at large β . In this regime, $X_{7\text{Li}}$ behaves differently, with its maximum variation occurring at an intermediate rather than the highest β . Overall, light-element abundances are more sensitive to the PBH fraction β than to the PBH mass M when $M > 10^{10}$ g, because the significant increase in the Hubble rate dominates over other effects. For very small PBH mass fractions ($\beta < 10^{-10}$), the effects on BBN are negligible.

At the threshold around $M \approx 10^{10}$ g, we examined how the reaction rates, Hubble expansion rate, and neutron-to-proton ratio collectively determine Y_{P} (from Fig. 9 to 11). For $M \geq 10^{10}$ g, the monotonic increase of Y_{P} with β is primarily driven by the accelerated Hubble expansion caused by PBH evaporation. In contrast, for $M \leq 10^{10}$ g, the relationship becomes non-monotonic, influenced by the timing of PBH evaporation and the role of β in modifying reaction rates. The interplay between these effects gives rise to the oscillatory dependence of Y_{P} observed in our simulations.

Large PBH fractions introduce additional challenges to our framework. Because PBHs behave as cold matter, their energy density scales as a^{-3} during cosmic expansion and can exceed that of the background radiation when $\beta(M) \approx 1$ at the onset of the simulation ($T = 30$ MeV). This situation would drive the universe into a matter-dominated phase, conflicting with our assumption of a homogeneous, isotropic, and radiation-dominated background. The associated growth of density inhomogeneities in such a regime cannot be captured within our current treatment. Therefore, while our framework successfully incorporates the key thermal and dynamical effects of PBHs on BBN, it does not account for the nonlinear evolution of large-scale inhomogeneities that may arise in a matter-dominated epoch.

Although our choice of $[n_s, dn_s/d\ln(k)]$ differs from the values inferred from CMB observations, it serves to illustrate how PBHs could influence the processes of BBN under alternative early-universe conditions. However, the qualitative effects of PBHs on BBN remain consistent with the mechanisms demonstrated in this work. By introducing an entropy injection mechanism through PBH evaporation, thereby allowing for scenarios that violate entropy conservation, we open a new path to explore how variations in entropy may reshape

other aspects of the thermal history of the universe. This framework provides a foundation for future studies examining the interplay between PBH evolution, thermal evolution, and the cosmological conditions that govern the early universe.

References

- [1] B. Carr, K. Kohri, Y. Sendouda and J. Yokoyama, *Constraints on primordial black holes*, *Rept. Prog. Phys.* **84** (2021) 116902 [[2002.12778](#)].
- [2] A.M. Green and A.R. Liddle, *Constraints on the density perturbation spectrum from primordial black holes*, *Phys. Rev. D* **56** (1997) 6166 [[astro-ph/9704251](#)].
- [3] C.T. Byrnes, E.J. Copeland and A.M. Green, *Primordial black holes as a tool for constraining non-Gaussianity*, *Phys. Rev. D* **86** (2012) 043512 [[1206.4188](#)].
- [4] H. Kodama, M. Sasaki and K. Sato, *Abundance of Primordial Holes Produced by Cosmological First Order Phase Transition*, *Prog. Theor. Phys.* **68** (1982) 1979.
- [5] F. Kühnel, C. Rampf and M. Sandstad, *Effects of Critical Collapse on Primordial Black-Hole Mass Spectra*, *Eur. Phys. J. C* **76** (2016) 93 [[1512.00488](#)].
- [6] H. Deng and A. Vilenkin, *Primordial black hole formation by vacuum bubbles*, *JCAP* **12** (2017) 044 [[1710.02865](#)].
- [7] H. Deng, J. Garriga and A. Vilenkin, *Primordial black hole and wormhole formation by domain walls*, *JCAP* **04** (2017) 050 [[1612.03753](#)].
- [8] T. Harada, C.-M. Yoo, K. Kohri, K.-i. Nakao and S. Jhingan, *Primordial black hole formation in the matter-dominated phase of the Universe*, *Astrophys. J.* **833** (2016) 61 [[1609.01588](#)].
- [9] C.-M. Yoo, T. Harada, J. Garriga and K. Kohri, *Primordial black hole abundance from random Gaussian curvature perturbations and a local density threshold*, *PTEP* **2018** (2018) 123E01 [[1805.03946](#)].
- [10] T. Harada, C.-M. Yoo, K. Kohri and K.-I. Nakao, *Spins of primordial black holes formed in the matter-dominated phase of the Universe*, *Phys. Rev. D* **96** (2017) 083517 [[1707.03595](#)].
- [11] K. Jedamzik, *Primordial black hole formation during the QCD epoch*, *Phys. Rev. D* **55** (1997) 5871 [[astro-ph/9605152](#)].
- [12] K. Jedamzik and J.C. Niemeyer, *Primordial black hole formation during first order phase transitions*, *Phys. Rev. D* **59** (1999) 124014 [[astro-ph/9901293](#)].
- [13] A. Polnarev and R. Zembowicz, *Formation of Primordial Black Holes by Cosmic Strings*, *Phys. Rev. D* **43** (1991) 1106.
- [14] R.R. Caldwell and P. Casper, *Formation of black holes from collapsed cosmic string loops*, *Phys. Rev. D* **53** (1996) 3002 [[gr-qc/9509012](#)].
- [15] E. Cotner, A. Kusenko, M. Sasaki and V. Takhistov, *Analytic Description of Primordial Black Hole Formation from Scalar Field Fragmentation*, *JCAP* **10** (2019) 077 [[1907.10613](#)].
- [16] E. Cotner and A. Kusenko, *Primordial black holes from supersymmetry in the early universe*, *Phys. Rev. Lett.* **119** (2017) 031103 [[1612.02529](#)].
- [17] B. Carr, F. Kühnel and M. Sandstad, *Primordial Black Holes as Dark Matter*, *Phys. Rev. D* **94** (2016) 083504 [[1607.06077](#)].
- [18] A.M. Green and B.J. Kavanagh, *Primordial Black Holes as a dark matter candidate*, *J. Phys. G* **48** (2021) 043001 [[2007.10722](#)].
- [19] B. Carr and F. Kühnel, *Primordial Black Holes as Dark Matter: Recent Developments*, *Ann. Rev. Nucl. Part. Sci.* **70** (2020) 355 [[2006.02838](#)].

- [20] S. Bird, I. Cholis, J.B. Muñoz, Y. Ali-Haïmoud, M. Kamionkowski, E.D. Kovetz et al., *Did LIGO detect dark matter?*, *Phys. Rev. Lett.* **116** (2016) 201301 [[1603.00464](#)].
- [21] K. Inomata, M. Kawasaki, K. Mukaida, Y. Tada and T.T. Yanagida, *Inflationary Primordial Black Holes as All Dark Matter*, *Phys. Rev. D* **96** (2017) 043504 [[1701.02544](#)].
- [22] S. Clesse and J. García-Bellido, *The clustering of massive Primordial Black Holes as Dark Matter: measuring their mass distribution with Advanced LIGO*, *Phys. Dark Univ.* **15** (2017) 142 [[1603.05234](#)].
- [23] J.R. Chisholm, *Clustering of primordial black holes: basic results*, *Phys. Rev. D* **73** (2006) 083504 [[astro-ph/0509141](#)].
- [24] G.M. Fuller, A. Kusenko and V. Takhistov, *Primordial Black Holes and r-Process Nucleosynthesis*, *Phys. Rev. Lett.* **119** (2017) 061101 [[1704.01129](#)].
- [25] Q.-f. Wu and X.-J. Xu, *Primordial Black Holes Evaporating before Big Bang Nucleosynthesis*, [2509.05618](#).
- [26] A. Boccia, F. Iocco and L. Visinelli, *Constraining the primordial black hole abundance through big-bang nucleosynthesis*, *Phys. Rev. D* **111** (2025) 063508 [[2405.18493](#)].
- [27] B. Carr and J. Silk, *Primordial Black Holes as Generators of Cosmic Structures*, *Mon. Not. Roy. Astron. Soc.* **478** (2018) 3756 [[1801.00672](#)].
- [28] G. Hasinger, *Illuminating the dark ages: Cosmic backgrounds from accretion onto primordial black hole dark matter*, *JCAP* **07** (2020) 022 [[2003.05150](#)].
- [29] B. Carr, S. Clesse, J. García-Bellido and F. Kühnel, *Cosmic conundra explained by thermal history and primordial black holes*, *Phys. Dark Univ.* **31** (2021) 100755 [[1906.08217](#)].
- [30] M.Y. Khlopov, S.G. Rubin and A.S. Sakharov, *Primordial structure of massive black hole clusters*, *Astropart. Phys.* **23** (2005) 265 [[astro-ph/0401532](#)].
- [31] M. Kawasaki, A. Kusenko and T.T. Yanagida, *Primordial seeds of supermassive black holes*, *Phys. Lett. B* **711** (2012) 1 [[1202.3848](#)].
- [32] B.J. Carr, K. Kohri, Y. Sendouda and J. Yokoyama, *New cosmological constraints on primordial black holes*, *Phys. Rev. D* **81** (2010) 104019 [[0912.5297](#)].
- [33] C. Keith, D. Hooper, N. Blinov and S.D. McDermott, *Constraints on Primordial Black Holes From Big Bang Nucleosynthesis Revisited*, *Phys. Rev. D* **102** (2020) 103512 [[2006.03608](#)].
- [34] M. Kawasaki, K. Kohri and T. Moroi, *Big-Bang nucleosynthesis and hadronic decay of long-lived massive particles*, *Phys. Rev. D* **71** (2005) 083502 [[astro-ph/0408426](#)].
- [35] A.M. Green, A.R. Liddle, K.A. Malik and M. Sasaki, *A New calculation of the mass fraction of primordial black holes*, *Phys. Rev. D* **70** (2004) 041502 [[astro-ph/0403181](#)].
- [36] A.R. Liddle and D.H. Lyth, *Cosmological inflation and large scale structure*, Cambridge (2000), [10.1017/CBO9781139175180](#).
- [37] B.J. Carr, *The Primordial black hole mass spectrum*, *Astrophys. J.* **201** (1975) 1.
- [38] B.J. Carr and S.W. Hawking, *Black holes in the early Universe*, *Mon. Not. Roy. Astron. Soc.* **168** (1974) 399.
- [39] T. Harada, C.-M. Yoo and K. Kohri, *Threshold of primordial black hole formation*, *Phys. Rev. D* **88** (2013) 084051 [[1309.4201](#)].
- [40] T. Harada and B.J. Carr, *Upper limits on the size of a primordial black hole*, *Phys. Rev. D* **71** (2005) 104009 [[astro-ph/0412134](#)].
- [41] M. Kopp, S. Hofmann and J. Weller, *Separate Universes Do Not Constrain Primordial Black Hole Formation*, *Phys. Rev. D* **83** (2011) 124025 [[1012.4369](#)].

- [42] C.R. Evans and J.S. Coleman, *Observation of critical phenomena and selfsimilarity in the gravitational collapse of radiation fluid*, *Phys. Rev. Lett.* **72** (1994) 1782 [[gr-qc/9402041](#)].
- [43] J.C. Niemeyer and K. Jedamzik, *Dynamics of primordial black hole formation*, *Phys. Rev. D* **59** (1999) 124013 [[astro-ph/9901292](#)].
- [44] I. Hawke and J.M. Stewart, *The dynamics of primordial black hole formation*, *Class. Quant. Grav.* **19** (2002) 3687.
- [45] I. Musco, J.C. Miller and L. Rezzolla, *Computations of primordial black hole formation*, *Class. Quant. Grav.* **22** (2005) 1405 [[gr-qc/0412063](#)].
- [46] S. Young, C.T. Byrnes and M. Sasaki, *Calculating the mass fraction of primordial black holes*, *JCAP* **07** (2014) 045 [[1405.7023](#)].
- [47] J.M. Bardeen, J.R. Bond, N. Kaiser and A.S. Szalay, *The Statistics of Peaks of Gaussian Random Fields*, *Astrophys. J.* **304** (1986) 15.
- [48] PLANCK collaboration, *Planck 2018 results. VI. Cosmological parameters*, *Astron. Astrophys.* **641** (2020) A6 [[1807.06209](#)].
- [49] E. Grohs, G.M. Fuller, C.T. Kishimoto and M.W. Paris, *Probing neutrino physics with a self-consistent treatment of the weak decoupling, nucleosynthesis, and photon decoupling epochs*, *JCAP* **05** (2015) 017 [[1502.02718](#)].
- [50] E. Grohs, G.M. Fuller and M. Sen, *Consequences of neutrino self interactions for weak decoupling and big bang nucleosynthesis*, *JCAP* **07** (2020) 001 [[2002.08557](#)].
- [51] B.V. Vainer and P.D. Nasel'skii., *Obvervable consequences of the evaporation of low-mass primordial black holes*, *Soviet Astronomy Letters* **3** (1977) 76.
- [52] B.V. Vainer, O.V. Dryzhakova and P.D. Nasel'skii., *Primordial black holes and cosmological nucleosynthesis*, *Soviet Astronomy Letters* **4** (1978) 185.
- [53] R.H. Cyburt, B.D. Fields, K.A. Olive and T.-H. Yeh, *Big Bang Nucleosynthesis: 2015*, *Rev. Mod. Phys.* **88** (2016) 015004 [[1505.01076](#)].
- [54] J. Bernstein, L.S. Brown and G. Feinberg, *COSMOLOGICAL HELIUM PRODUCTION SIMPLIFIED*, *Rev. Mod. Phys.* **61** (1989) 25.
- [55] V.F. Mukhanov, *Nucleosynthesis without a computer*, *Int. J. Theor. Phys.* **43** (2004) 669 [[astro-ph/0303073](#)].
- [56] K. Jedamzik, *The cosmic Li-6 and Li-7 problems and BBN with long-lived charged massive particles*, *Phys. Rev. D* **77** (2008) 063524 [[0707.2070](#)].
- [57] M. Asplund, D.L. Lambert, P.E. Nissen, F. Primas and V.V. Smith, *Lithium isotopic abundances in metal-poor halo stars*, *Astrophys. J.* **644** (2006) 229 [[astro-ph/0510636](#)].
- [58] F. Iocco, *The lithium problem, a phenomenologist's perspective*, *Mem. Soc. Astron. Ital. Suppl.* **22** (2012) 19 [[1206.2396](#)].
- [59] E.W. Kolb and M.S. Turner, *The Early Universe*, vol. 69, Taylor and Francis (5, 2019), [10.1201/9780429492860](#).
- [60] M. Peimbert, A. Peimbert and M.T. Ruiz, *The chemical composition of the Small Magellanic Cloud H II region NGC 346 and the primordial helium abundance*, *Astrophys. J.* **541** (2000) 688 [[astro-ph/0003154](#)].
- [61] E. Aver, K.A. Olive and E.D. Skillman, *The effects of He I $\lambda 10830$ on helium abundance determinations*, *JCAP* **07** (2015) 011 [[1503.08146](#)].
- [62] D. Tytler, J.M. O'Meara, N. Suzuki and D. Lubin, *Review of Big Bang nucleosynthesis and primordial abundances*, *Phys. Scripta T* **85** (2000) 12 [[astro-ph/0001318](#)].

- [63] F. Iocco, G. Mangano, G. Miele, O. Pisanti and P.D. Serpico, *Primordial Nucleosynthesis: from precision cosmology to fundamental physics*, *Phys. Rept.* **472** (2009) 1 [[0809.0631](#)].
- [64] R.J. Cooke, M. Pettini and C.C. Steidel, *One Percent Determination of the Primordial Deuterium Abundance*, *Astrophys. J.* **855** (2018) 102 [[1710.11129](#)].
- [65] M. Kawasaki, K. Kohri, T. Moroi and Y. Takaesu, *Revisiting Big-Bang Nucleosynthesis Constraints on Long-Lived Decaying Particles*, *Phys. Rev. D* **97** (2018) 023502 [[1709.01211](#)].
- [66] T.M. Bania, R.T. Rood and D.S. Balsler, *The cosmological density of baryons from observations of $3\text{He}+$ in the Milky Way*, *Nature* **415** (2002) 54.
- [67] S.G. Ryan, T.C. Beers, K.A. Olive, B.D. Fields and J.E. Norris, *Primordial Lithium and Big Bang Nucleosynthesis*, *Astrophys. J. Lett.* **530** (2000) L57 [[astro-ph/9905211](#)].
- [68] B.D. Fields, *The primordial lithium problem*, *Ann. Rev. Nucl. Part. Sci.* **61** (2011) 47 [[1203.3551](#)].
- [69] S.W. Hawking, *Particle Creation by Black Holes*, *Commun. Math. Phys.* **43** (1975) 199.
- [70] J.H. MacGibbon, *Quark and gluon jet emission from primordial black holes. 2. The Lifetime emission*, *Phys. Rev. D* **44** (1991) 376.
- [71] C. Lunardini and Y.F. Perez-Gonzalez, *Dirac and Majorana neutrino signatures of primordial black holes*, *JCAP* **08** (2020) 014 [[1910.07864](#)].
- [72] F. Halzen and A.D. Martin, *QUARKS AND LEPTONS: AN INTRODUCTORY COURSE IN MODERN PARTICLE PHYSICS*, Wiley (1984).
- [73] B.J. Carr, *Some cosmological consequences of primordial black-hole evaporations*, *Astrophys. J.* **206** (1976) 8.
- [74] M. He, K. Kohri, K. Mukaida and M. Yamada, *Formation of hot spots around small primordial black holes*, *JCAP* **01** (2023) 027 [[2210.06238](#)].
- [75] S. Dodelson and F. Schmidt, *Modern Cosmology*, Academic Press (2020), [10.1016/C2017-0-01943-2](#).
- [76] S.K. Acharya and R. Khatri, *CMB and BBN constraints on evaporating primordial black holes revisited*, *JCAP* **06** (2020) 018 [[2002.00898](#)].
- [77] M.E. Burbidge, G.R. Burbidge, W.A. Fowler and F. Hoyle, *Synthesis of the elements in stars*, *Rev. Mod. Phys.* **29** (1957) 547.